Chandra LETG higher order diffraction efficiencies

B.J. Wargelin, P.W. Ratzlaff, D.O. Pease, V.L. Kashyap, and J.J. Drake

Smithsonian Astrophysical Observatory, Cambridge MA 02138, USA

ABSTRACT

Accurate calibration of the *Chandra* Low Energy Transmission Grating (LETG) higher-order ($|m| > 1$) diffraction efficiencies is vital for proper analysis of spectra obtained with the LETG's primary detector, the HRC-S, which lacks the energy resolution to distinguish different orders. Pre-flight ground calibration of the LETG was necessarily limited to sampling a relatively small subset of spectral orders and wavelengths, and virtually no higher-order data are available in the critical region between 6 and 10 Å. In this paper, we describe an analysis of diffraction efficiencies based on in-flight data obtained using the LETG's secondary detector, the ACIS-S. Using ACIS, the *relative* efficiency of each order can be studied out to $|m\lambda| \sim 80$ Å, which is nearly one-half of the LETG/HRC-S wavelength coverage. We find that the current models match our results well but can be improved, particularly for the even orders just longward of the Au-M edge at 6 Å.

Keywords: Chandra, LETG, diffraction efficiency, calibration

1. INTRODUCTION

Most of the effort on calibration of LETG diffraction efficiencies has been spent on analyzing ground calibration data collected during the winter of 1996/97 at the X-Ray Calibration Facility (XRCF) at Marshall Space Flight Center (MSFC) in Huntsville, AL. The most extensive and cleanest data set is from the Electron Impact Point Source (EIPS), which was collected using a set of Flow Proportional Counters (FPCs). The EIPS emits photons primarily in one or more strong lines which are characteristic of the anode material used; the energies used during calibration range from 108 eV (Be-Kα) to 8041 eV (Cu-Kα). Because the EIPS only provides photons at specific energies, however, energy coverage is inherently incomplete, and is particularly poor between 6 and 12 Å (2 and 1 keV), where grating efficiency varies substantially with energy (see Fig. 1). In addition, higher-order efficiencies (2nd, 3rd, etc.) were calibrated at only a handful of energies.

Additional ground calibration data are available (using various combinations of monochromators and flight or ground detectors), but these data are generally more difficult to analyze and have larger systematic uncertainties than the EIPS data, which were already very complicated to analyze (Wargelin et al, in preparation). Flight data can also be used, but LETG spectra are usually collected with the High-Resolution Camera–Spectroscopy (HRC-S), which has high background and effectively no energy resolution for order separation, so that higher-order efficiencies can only be derived at a few energies where there are strong lines.

In contrast, the LETG's secondary detector, the Advanced CCD Imaging Spectrometer–Spectroscopy (ACIS-S) provides easy order separation at most energies because of its intrinsic energy resolution. Less than half of the LETG/HRC-S wavelength range is covered by the shorter ACIS-S detector, but its useful range includes the shorter wavelengths where grating efficiencies vary most strongly. As with any analysis of flight data, we are limited by imperfect knowledge of the true astrophysical source spectrum and intensity, but *relative* grating efficiencies, e.g., 2nd/1st, can be measured quite accurately. This paper describes our analysis and results from several LETG/ACIS-S observations, and discusses our plans for further calibration of LETG diffraction efficiencies.

Figure 1. LETG efficiencies from ground calibration at XRCF, using Electron Impact Point Source data. Smaller red symbols mark cases where model HRMA effective area predictions were used in lieu of unavailable grating-out measurements. Higher-order calibration was sparse, but seems to indicate some disagreements with current calibration model predictions (continuous lines).

2. DATA SELECTION

To obtain high-quality results we need a lot of counts. Emission line sources provide high-count data at discrete energies, but those lines often suffer from detector pile-up (see Sect. 4). Pile-up can be modeled, but this is very difficult for line spectra because event distribution varies so strongly along the dispersed spectrum. It is much easier to correct for pile-up with a smoothly varying spectrum, as with a continuum source, and the energy coverage is by definition continuous. Pile-up is minimal in dim spectra, but counting statistics will be worse and detector background may be a significant complication. As long as pile-up can be adequately corrected, the best LETG/ACIS-S flight data to use are therefore long exposures of bright continuum sources.

Using these criteria, along with a preference for data collected using a short ACIS frame-time to minimize pile-up (0.7 s for all the observations studied here), the sources we selected for this calibration are:

- "SourceX," a proprietary observation with the highest counting rate and largest number of counts.

- XTEJ1118+480 (obsid 1701, 22 ks), a very bright X-ray nova.

- PKS 2155-304, observed several times as a calibration target. We used obsid 3669, a 42-ks observation obtained when PKS 2155-304 was particularly bright.

Source spectra are shown in Fig. 2. Data from 3C 273 and shorter/dimmer observations of PKS 2155-304 were also analyzed. Results are fully consistent with those from the brighter sources but of poorer statistical quality, and are not discussed further.
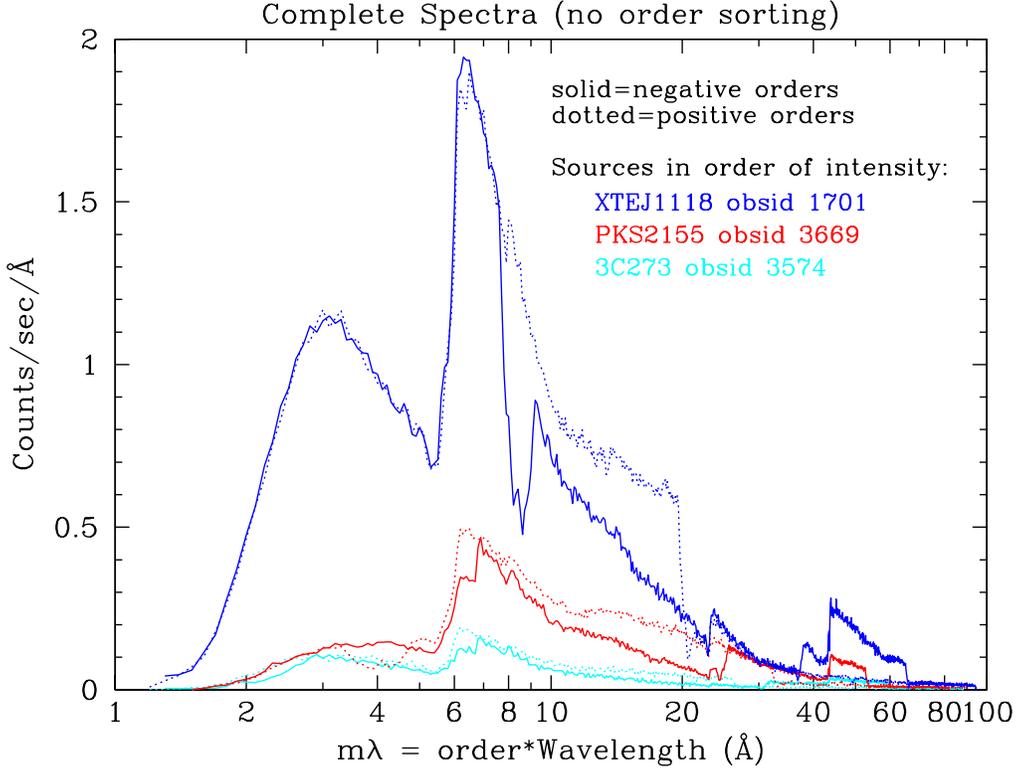
Figure 2. Spectra used in this analysis, showing widely varying rates. The SourceX spectrum is not shown, as the data are still proprietary, but the source is more than 50% brighter than XTEJ1118. Analysis results from 3C 273 are not shown in subsequent figures, as the data points have very large statistical error bars.

3. ANALYSIS METHOD

For each observation, we start with the level 1.5 event file, which has the `tg_mlam` ($m\lambda$) column. GTI time filtering is then applied, along with standard status-bit filtering, with the exception of status-bit 5 (the adjacent badpix test); we argue that this filtering should not be used on grating data because it removes entire columns of only marginal "badness" that have already been well-filtered according to their dispersed energy. The position of 0th order, used to determine `tg_mlam` values, is also checked, as automatic pipeline processing can be thrown off when the inner cores of very bright sources are piled-up.

Spectral data are extracted from within 3.3-degree-wide sectors along the dispersion axis (see Fig. 3). The angular width is chosen to exclude secondary diffraction from the fine-support structure in the cross-dispersion direction, while also including nearly all the flux dispersed by the coarse-support structure. Net extraction efficiency is approximately 90% with negligible dependence on wavelength. Data near 0th order ($|m\lambda| < 1.2$ Å) are excluded because of substantial contamination by high-energy scattered photons.

The heart of this analysis is the extraction of narrow slices of spectrum (more than 700) with corresponding higher orders up to $|m| = 7$, excluding chip gaps and wavelength ranges near them that are affected by spacecraft dither. For example, we extract a slice of $m\lambda = 2.0 - 2.1$ Å for +1st order, $m\lambda = 4.0 - 4.2$ Å for +2nd order, $6.0 - 6.3$ Å for +3rd order, and so on, for negative orders as well. This ensures that we are comparing the number of events in different orders from exactly the same part of the emitted spectrum (same wavelength λ, same energy). The width of each slice, $\Delta\lambda$, is chosen to collect a statistically significant number of counts in each order, but $\Delta\lambda$ cannot be too large or events from different orders within the corresponding area on the detector will overlap in energy space and prevent effective order separation.
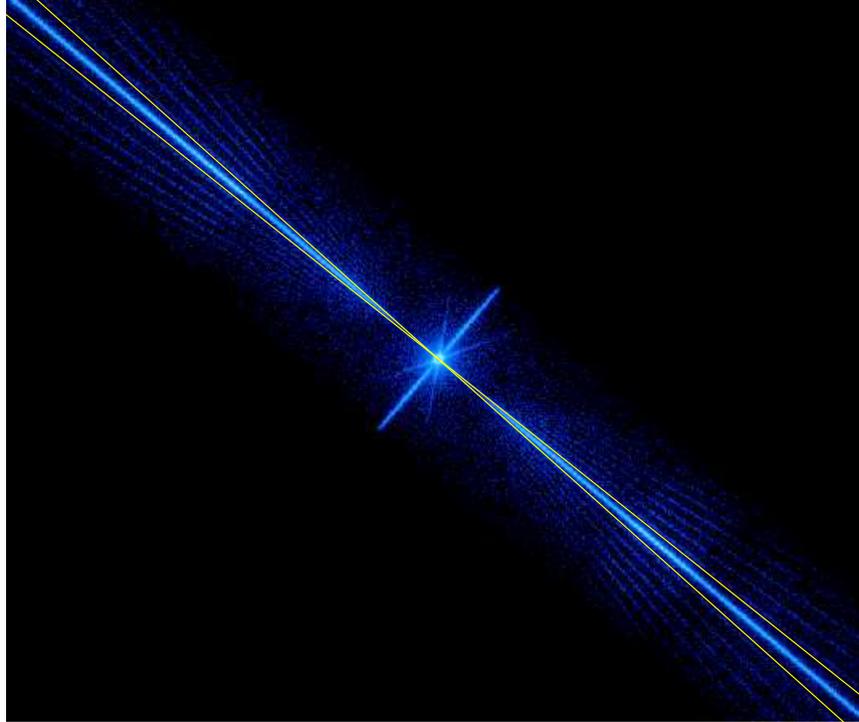
Figure 3. Image of XTEJ1118 dispersed spectrum, showing secondary diffraction and the spectral extraction region (yellow). The sector-shaped extraction region was chosen to maintain a constant extraction efficiency (90%) as a function of wavelength.

For each spectral slice, we then determine the number of counts in order m based on that slice's energy pulse-height spectrum (see Fig. 4). Ideally, full spectral fitting using detector response matrices would be used for each data slice, but the thousands of fits required for each observation make this approach impractical. Instead, we use a simple region-of-interest (ROI) analysis, calculating the range of pulse-height-invariant (PI) values for each order based on the range of dispersed photon energies within each slice of spectrum. To calculate the ROI limits, we first determine the energy range corresponding to the range of λ and then shift those energies, E_{low} and E_{high}, down by 2.0 and 1.5 PI channels (29.2 and 21.9 eV, respectively) to account for the slightly nonsymmetrical shape of the ACIS energy response function.

The width of the response function, w, is equal to the quadrature sum of the electronic noise and energy-dependent Fano broadening, which we approximate as

$$w = \sqrt{(110\ \mathrm{eV})^2 + 36E_{ave}}, \tag{1}$$

where E_{ave} is the average of E_{low} and E_{high} in eV. ROI limits for PI are then given by

$$PI_{low} = (E_{low} - \frac{1}{2}w)/14.6 \quad \text{and} \quad PI_{high} = (E_{high} + \frac{1}{2}w)/14.6 \tag{2}$$

rounded to the nearest integer. At energies just above the Si-K absorption edge at 1839 eV, PI values are adjusted downward (3 channels for $E = 1839 - 2100$ eV, 2 channels for $E = 2100 - 2500$ eV, and 1 channel for $E = 2500 - 3000$ eV) to account for a jump in the work function across the edge. The number of counts in order $m - 1$ and in 1st order, as well as the total number of counts in the spectral slice, are also determined in order to apply pile-up corrections (Sect. 4) and determine the "true" number of counts within each diffracted order for a given wavelength. Diffracted orders are dispersed across the ACIS-S array of six CCDs, so QE-corrected counting rates must also be determined. The statistically weighted counting rate average of the positive and
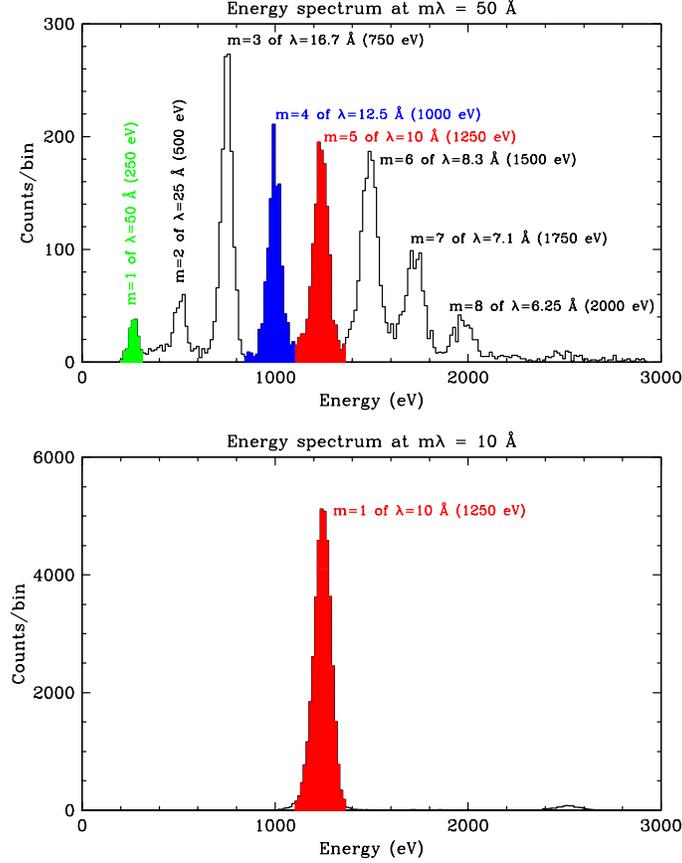
Figure 4. Example energy spectra. Top panel is for the wavelength range $m\lambda = 49.0$ to 50.5 Å. Colored shading shows which peaks are used to determine the pile-up-corrected number of counts in 5th order of 10 Å. The total number of counts in the entire spectrum is also used in pile-up calculations (see Eqs. 3 and 4). In this example, pile-up corrections are negligible. For comparison, the 1st order spectrum of 10 Å (used in calculation of the 10-Å 5th/1st efficiency ratio) is shown in the bottom panel.

negative orders are computed for each m, and finally the adjusted rate for each higher order relative to 1st order is calculated. Results are shown in Figs. 5–10, with and without pile-up corrections. Note that for consistency, the vertical scale on each plot always spans a factor of 20 (except for 2nd order, which uses a slightly larger range).

4. PILE-UP CORRECTIONS

When two or more X rays are collected by ACIS within a 3×3-pixel "event island" during a single frame (0.7 seconds for LETG/ACIS spectra collected using a 1/8 subarray, but up to 3.2 s for the full array), they will either be counted as a single event having an energy equal to the sum of the two events' energies, or will be discarded as an invalid event, depending on which pixels within the 3×3 island are activated. The first case is associated with the parameter k_p (for *p*ileup) and the second case with k_g (for bad-*g*rade losses). The most obvious evidence of pile-up is in 2nd order below 6 Å (see top panel of Fig. 5). The large bump in the 2nd/1st ratio between roughly 3 and 5 Å arises from the pile-up of 1st-order photons between 6 and 10 Å, while the smaller bump below ~ 3 Å is from pile-up of 1st-order photons around 3 Å(see Fig. 2).

For 1st order, the true and *obs*erved counting rates are approximately related by

$$r_1^{obs}(\lambda) = r_1(\lambda) - 2(k_p + k_g)r_1(\lambda)r_1(\lambda) - (k_p + k_g)r_1(\lambda)r_{all\ but\ 1}, \tag{3}$$
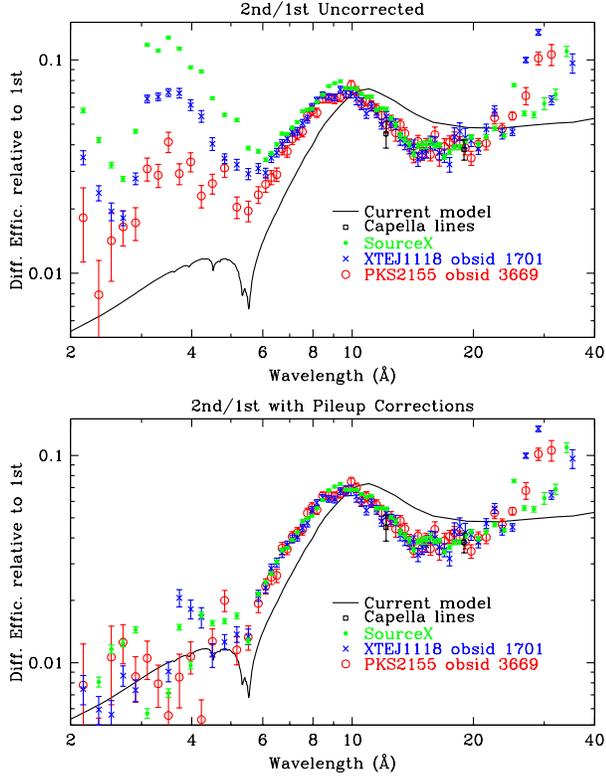
Figure 5. Ratio of 2nd and 1st-order efficiencies, showing results without pile-up corrections (top panel) and with corrections (bottom). Pile-up of 1st-order events is obvious below 6 Å. Points beyond ~ 20 Å are spurious; the 2nd-order energy-spectrum peak cannot be cleanly separated using ROI analysis from the stronger 3rd-order peak.

Figure 6. Ratio of 3rd and 1st-order grating efficiencies. Agreement with the current model is very good, but can be improved by roughly 10% at wavelengths beyond ~ 8 Å. Beyond the "bump", data from line sources collected with the HRC-S will be important in calibrating the longer-wavelength efficiencies.

where $r_{all\ but\ 1}$ means the rate for all orders except 1st in that slice of spectrum. The coefficient for the $(k_p + k_g)r_1(\lambda)r_1(\lambda)$ term is 2 because two 1st-order events are lost from the 1st-order peak when they pile up with each other, whereas only one 1st-order event is lost when it piles up with any other event (corresponding to the last term in Eq. (3)).

For higher orders, the equation is

$$r_m^{obs}(\lambda) = r_m(\lambda) + k_p r_{m-1}(\frac{m}{m-1}\lambda)r_1(m\lambda) - (k_p + k_g)r_m(\lambda)r_{all}, \qquad (4)$$

where the $k_p r_{m-1}(\frac{m}{m-1}\lambda)r_1(m\lambda)$ term corresponds to order $m-1$ events piling up with 1st order events to create additional apparent order m events. The last term is for pile-up of m-order events with any event, leading to the loss of those events from the mth order.

When discussing pile-up in dispersed spectra, rates are most naturally given in units of counts/dispersion-pixel/frame. From empirical study of 2nd-order results below 6 Å, where the apparent 2nd-order flux is mostly from 1st-order pile-up, we find that k_p is between 0.45 and 0.70 pixel·frame/count, with a best value of 0.56 pixel·frame/count. (Preliminary work indicates that k_p is somewhat larger for front-illuminated ACIS chips and smaller for back-illuminated chips, but the only significant impact on the results presented here is improved consistency of 2nd-order results at wavelengths shorter than 6 Å.) For dispersed spectra, k_g is approximately $0.7k_p$ (and likely also differs for FI and BI chips). Iteratively solving the equations above, we determined the true (unpiled) rates for each order.
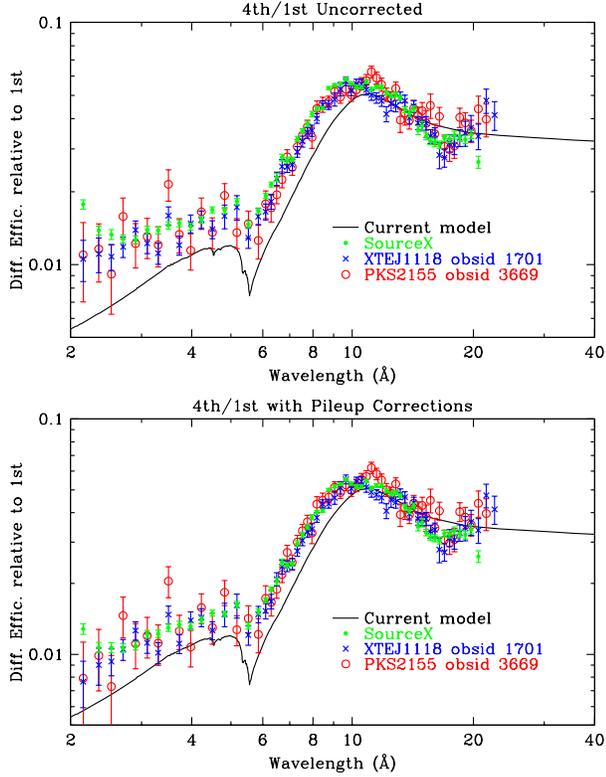
Figure 7. Ratio of 4th and 1st order efficiencies. Longward of ~ 15 Å, ROI analysis cannot adequately separate the 4th- and 3rd-order energy-spectrum peaks.
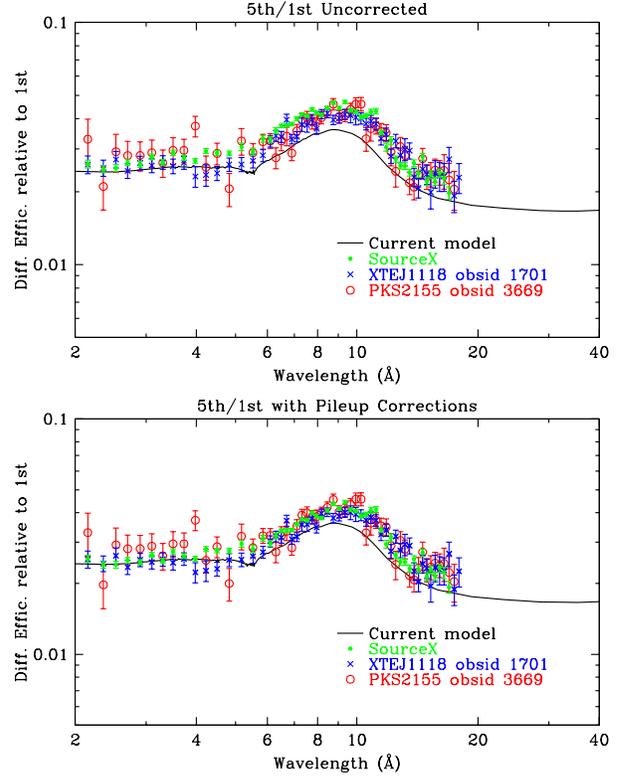
Figure 8. Ratio of 5th and 1st-order efficiencies. Current model appears to be $\sim 15\%$ low at most wavelengths, but the overall agreement in shape is good.

In the worst case, for SourceX around 6.5 Å, the pile-up fraction of 1st-order events ($k_p r_1$) is $\sim$12%, which corresponds to a net loss of events from the 1st-order spectrum ($2(k_p + k_g)r_1$–see Eq. (3)) of $\sim$40%. To first order, however, pile-up losses mostly cancel out when determining relative efficiencies, so that the net effect of pile-up corrections in our calibration is minor or negligible, except for 2nd order at short wavelengths where diffraction efficiency is very low.

5. CONCLUSIONS

Although absolute grating efficiencies cannot be determined using in-flight data, this analysis has shown that high-quality calibration results can be obtained on relative higher-order efficiencies. Pile-up in high-intensity sources is a complication, but can be quite accurately accounted for, as evidenced by the excellent agreement we obtain in results from different data sets with counting rates that vary by an order of magnitude. Although improvements can and will be made to our analysis, a number of important conclusions can already by drawn.

Probably the most important is that the current model of the relative efficiency of 3rd order, the most important higher order, is quite good, with errors of no more than 10 or 15% at any wavelength. Given the size of the error bars, a calibration accuracy of order 5% should be achievable. Furthermore, based on results from 5th and 7th order, it appears that the relative efficiencies of other odd orders also agree well with current models, but are underpredicted by $\sim$15%.

Model agreement with even orders is not as good, particularly with respect to the shape of the Au-M edge "bump" between 6 and 12 Å (2 and 1 keV). This may indicate that the model shape for all orders, including 1st, needs improvement. Beyond $\sim$15 Å, the 2nd order model overpredicts relative efficiency by $\sim$30%, and 4th order is also overpredicted, by $\sim$20%. These results must be confirmed with more detailed analysis (because of
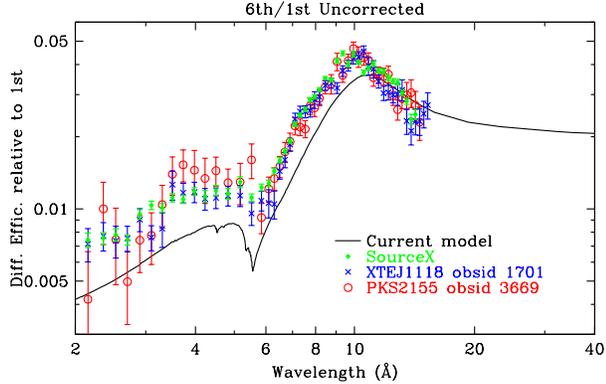
Figure 9. Ratio of 6th and 1st order efficiencies.
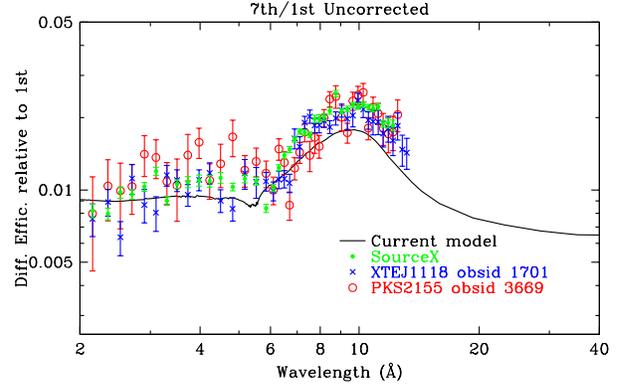
Figure 10. Ratio of 7th and 1st-order efficiencies.
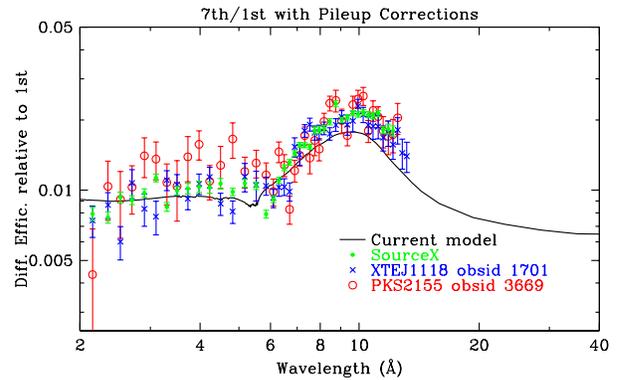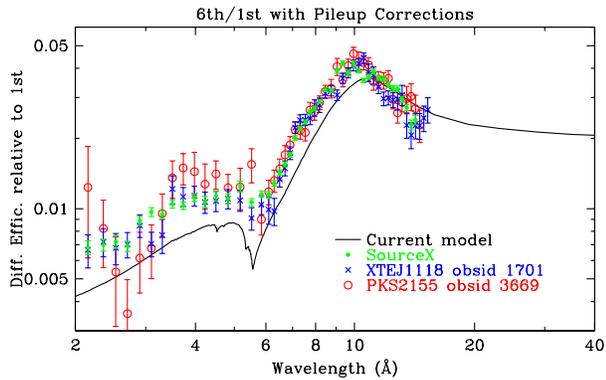
order-separation difficulties in ACIS spectra at low energies) and results from LETG/HRC-S data, but if correct, such errors may sometimes be important since 2nd and 4th order are not much weaker than 3rd order.

6. FUTURE WORK

To take full advantage of our relative-efficiency calibration we we must improve our knowledge of the absolute 1st order efficiency. This is a more difficult task: cosmic sources do not have absolutely calibrated spectra, and XRCF EIPS data do not map out the shape of the Au-M bump, where grating efficiency varies strongly with wavelength, and is at a maximum (for odd orders). There are additional XRCF ground-calibration data which can be used for this purpose, but their systematic uncertainties are larger than for the EIPS measurements and the data are more difficult to analyze for a variety of reasons. We are currently analyzing Double Crystal Monochromator (DCM) data collected with the FPC ground-calibration detectors, and may attempt analysis of LETG/HRC-S data (collected with pre-flight detector settings).

The other main limitation of our work is that it only covers a fraction of the LETG/HRC-S wavelength range. Following completion of the LETG/ACIS-S analysis we will next analyze bright lines in LETG/HRC-S spectra to extend coverage to lower energies. The HRC's higher detector background and the inability to separate orders based on intrinsic detector energy resolution means, however, that uncertainties will be relatively large, and the number of bright lines at long wavelengths is limited. Helpfully, however, grating efficiencies are nearly flat over a wide range of wavelengths beyond ~ 15 Å so that we should be able to obtain accurate average values.

As for the work on LETG/ACIS-S data described here, there are several improvements that can be made for our final reanalysis:

- Wavelength slices should be made narrower at the shortest wavelengths to avoid order overlap.

- Values of k_p and k_g should be more rigorously determined, with different values for FI and BI chips, and perhaps have energy dependence.

- Equations for calculation of ACIS energy resolution and ROIs can be improved, such as differentiating between FI and BI chips.

- The accuracy of pile-up corrections can be improved by including more terms. Also, current error estimates do not fully account for uncertainties in the pile-up corrections.

- The spectral extraction efficiency of the sector spatial filter has a relative uncertainty believed to be less than a few percent, but this should be better quantified.

- At long wavelengths, the pulse-height peaks of weak orders merge with the shoulders of stronger adjacent peaks, so our simple region-of-interest analysis fails (see the rising tails in the 2nd and 4th order plots). Spectral fitting could be used to extend the useful range of the LETG/ACIS analysis.

- When comparing orders falling on different ACIS chips, relative QE errors must be considered. Conversely, one can use this type of analysis to better calibrate the relative QEs of the ACIS chips, as noted by Marshall (`http://space.mit.edu/ASC/calib/letg_acis/letg_acis_cal.ps.gz`).

- More generally, comparisons between results for positive and negative orders should be studied more closely.